Geometric Quantification of Tendon Second Harmonic Images

Ann K Harvey[a,c*], Mark S Thompson[b], Zhanfeng Cui[b] and Sir Michael Brady[a]

[a]Wolfson Medical Vision Laboratory, Department of Engineering Science, University of Oxford, Oxford.
[b]Institute of Biomedical Engineering, Department of Engineering Science, University of Oxford, Oxford.
[c]Life Sciences Interface Doctoral Training Centre, University of Oxford, Oxford.

Abstract. Tendons are composed of cells, blood vessels and extracellular matrix, intricately woven together to form a vital musculoskeletal connective tissue. There is a growing need for functional imaging of tendon, for example to provide non-invasive biochemical and biomechanical insight into injured, diseased or repairing tendon. This study describes the possibility of developing an magnetic resonance imaging (MRI) tool for tissue quality assessment. Near infrared-multiphoton laser scanning microscopy (NIR-MPLSM) was used to validate ultra-high field MRI-based distinctions between normal and damaged tendon. Using a novel interpretation framework based on intrinsic tissue geometry, tissue damage at the matrix level was quantified according to local and global geometric parameters. The tendon characteristic crimp waveform and matrix geometric regularity were disrupted by enzyme-digestion, potentially compromising the tissue mechanical properties. These findings suggest that different imaging modalities can reveal complementary and corresponding information about tendon structures at functionally relevant scales. The proposed framework provides a robust and quantifiable physiological description of tendon, which can be exploited for clinical tendon tissue classification, and related to *in vivo* MR imaging.

1 Introduction

Connective tissues constitute vital components of the musculoskeletal system; tendons enable skeleton movement by transmitting forces created in muscles to bones, and ligaments connect bones to each other. Tendons and ligaments suffer from a wide range of clinical problems, including rupture and degenerative pathology. The anterior cruciate ligament (ACL) rupture is an injury resulting from abnormal mechanical loading at the knee, often incurred during sporting activity. The estimated incidence of ACL rupture is 30 per $100,000$ of the general population [1], but the incidence in athletes is much higher.

The most common treatment for ACL rupture patients is surgical reconstruction, whereby a tendon graft is used to replace the damaged ACL. Success rate, however, is variable with successful long-term results achieved in only 75-95% of cases [2]. For successful outcome, the tendon graft must adapt to the its biochemical and mechanical environment, a process known as tendon ligamentisation [3]. Since these remodeling processes are not yet well understood, it is difficult to pin-point the cause of tendon graft failure. Non-invasive imaging techniques may provide insight into these underlying physiological mechanisms, and therefore address the growing demand for methods to functionally explore musculoskeletal tissue *in vivo*. The full potential of magnetic resonance imaging (MRI) in tendon imaging has scarcely been realised. This is perhaps because the MR signal intensity from tendons acquired using most clinical protocols is low, making it difficult to extract meaningful information from these signal voids. Specific MRI protocols, for example using ultra-high magnetic field, contrast agent, or ultra-short echo time (UTE), may in time provide insight into underlying physiological processes.

Tendons comprise cells, blood vessels and extracellular matrix (ECM), where collagen (65-80% dry weight), elastin (1-2% dry weight) and proteoglycans (PGs) (0.2-5.0% dry weight) are located [4]. The ECM provides structural support for cells, occupies the intracellular space and helps provide mechanical support by buffering tensile and compressive tissue strains. Despite the small percentage of ECM occupied by PGs, they can hold water about 50 times their weight. For example, chondroitin sulphate (CS) is an abundant tendon GAG involved in regulating fibrillogenesis (fibril formation and development), fibril diameter, and cell proliferation.

The abundance of collagen makes tendon an excellent candidate for the endogenous nonlinear excitation process called second harmonic generation (SHG). SHG of longitudinally sectioned tendon reveals the functionally important crimping waveform characterised by alternating periodic light and dark bands (Figure 1(C)). This is typically demonstrated by polarised light microscopy or near infrared-multiphoton laser scanning microscopy (NIR-MPLSM), the latter of which enables collection of image stacks of different coloured channels much like confocal microscopy.

The SHG tendon representation yields intrinsic structural information about the microstructural organisation, including local edges related to cimping. Therefore, analysis of SHG images provides a potential tool for visualising the pathological tissue damage, and monitoring the healing processes of repair. Quantitative interpretation of SHG images may

*Corresponding author: Ann K Harvey, Email: harvey@robots.ox.ac.uk.

help determine imaging parameters which can be used to classify normal or damaged tendon. We propose a novel interpretation framework for extracting functional parameters relating to the crimp waveform and global organisation of the tissue. Figure 1 shows the representation of each image plane as a surface comprising families of curves with constant u (fibre direction) and v (light/dark banding pattern). This intrinsic framework can be fitted to the SHG images.

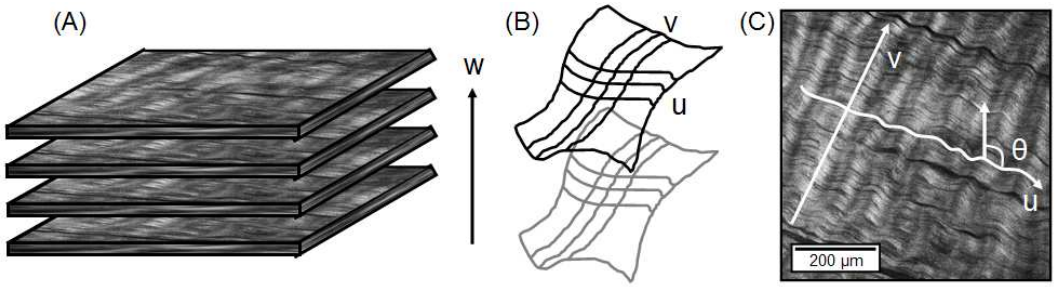

Figure 1. (A) The SHG image stack. (B) Surface representation comprising families of curves with constant u and v, and image plane index, w. (C) Intrinsic tissue co-ordinates u and v, represent local fibre orientation (at angle, θ) and fibre banding pattern, respectively.

We have previously shown that MRI signal can be correlated with histological staining and NIR-MPLSM imaging of functionally important tendon proteins [5]. This study is focussed on imaging normal and damaged (enzyme-digested) tendon samples, and is aimed at providing a physiological understanding of the signals produced by MRI. The MRI work is validated by quantifiable NIR-MPLSM, in an attempt to show the potential of MRI for tendon clinical tissue assessment.

2 Methods

2.1 Image Acquisition

Extracted adult bovine lower limb tendon samples were incubated in phosphate buffered saline (PBS), or enzyme-containing buffer (papain, trypsin, collagenase) for 16 hours at 37°C. NIR-MPLSM tendon samples were embedded in paraffin, sectioned, and stained using primary (chondroitin sulphate (CS)-56, Sigma) and secondary (AlexaFluor-488, Invitrogen) antibodies.

NIR-MPLSM. A NIR-MPLSM system was employed to image tendon sections, embedded in paraffin. The system consists of a diode pumped Ti:Sapphire crystal laser (Mira-Coherent, Ely, UK) coupled to a BioRad Radiance 2100 MPD laser-scanning system (Carl Zeiss GmbH, Germany) and a Nikon E600 FN upright microscope (Nikon UK Ltd, UK). Laser excitation was conducted at 800 nm. SHG emissions were captured by a blue filter ($400 - 430$ nm); AlexaFluor-488 emissions were captured by a green filter ($500-530$ nm). Images were quantified using custom-written scripts in MATLAB R2008b.

MRI. MR imaging was carried out using a 300 MHz horizontal bore 7 Tesla magnet interfaced to a Varian Inova console (Varian Inc., Palo Alto, CA) using a transmit receive quadrature birdcage coil (55 mm) diameter. T2-weighted imaging was performed using a fast spin echo sequence with a repetition time (TR) of 0.3 s and an echo spacing (TE) of 0.015 s. T1-weighted imaging was performed using a fast spin echo sequence with TR 0.1 s and TE 0.0125 s.

2.2 Image Analysis

Three regions of normal and enzyme-digested SHG images were analysed to quantify functional ECM parameters.

Local geometry. To estimate local u co-ordinates in the fibre direction, the following method was used: image rotation, Fourier-based low band-pass filtering in the y-direction (x-oriented edges) and x-direction (y-oriented edges), Canny edge detection (see [6] for details) and spline curve fitting. Spline curves, $\mathbf{S}$, were fitted to the edges as defined by more than 20 connected pixels, m:

$$\mathbf{S}(x) \;=\; \sum_{i=1}^{m} P_i\, \bar{k}_i(x) \quad : \; m > 20, \tag{1}$$

where the control points, P_i, are defined by the edge co-ordinates. The crimp waveform wavelength and amplitude, as

estimated from the local maxima and minima of the spline curves, were estimated from the y-oriented edges. Tissue curvature, κ, deviation from a straight line, was estimated using differential geometry, the Frenet-Serret equations [7].

Global organisation. To estimate the global tissue organisation, the intensity variation across small image windows was quantified. The rotation angle, θ, giving rise to the minimum summed intensity variance over window rows, σ, was computed for every pixel (x, y):

$$\Theta(x,y) \;=\; \min_{\theta=0}^{180} \left(\sum_{r=1}^{n} \sigma(\bar{Y}_r) \right), \tag{2}$$

where $\bar{Y}$ is a vector of intensity values across a row, r, of the sampling window, with dimensions $n \times n$, where $n = 5, 7$ or 9 pixels. Summed variances were calculated based on a 22.5° sampling of the rotation angle, $\theta = \{0^\circ, 22.5^\circ, ..., 180^\circ\}$, where θ is measured as clockwise deviation from the y-axis (Figure 1(C)). The angle of minimum intensity variation results were plotted in the form of a histogram, and the order (geometric regularity), Δ, of the sample was estimated using the sum of squares:

$$\Delta \;= \sum_{i=1}^{n} (\chi - \bar{\chi})^2, \tag{3}$$

where $\bar{\chi}$ and χ are the number and mean number of elements in each angle bin, respectively, and $n = 5, 7$ or 9 number of possible rotation angles. Tissue order, Δ, was normalised against the PBS-incubated sample, which was assigned $\Delta = 1$.

3 Results and Discussion

3.1 Local Geometry

The fibre tracking method exploits implicit information about fibre orientation from the tissue boundaries, to determine local estimates of u and v. Canny edge detection reveals the x- (Figure 2(B)) and y-oriented (Figure 2(C)) edges, which manifest at different spatial scales, and consequently highlight different tissue features. The y-oriented edges were fitted to spline curves, which represent local fibre tracking and specifically the u co-ordinate of the intrinsic framework (Figure 2(D)).

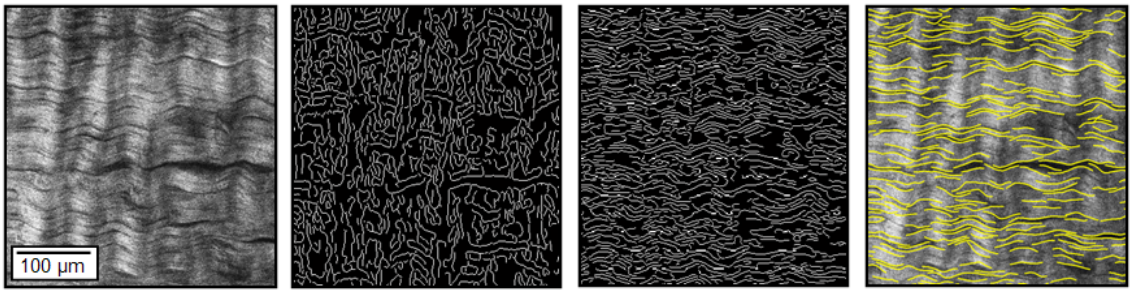

Figure 2. Raw image intensities (A). Edges determined by Canny edge detection after low band-pass filtering with horizontal (B) and vertical (C) filter. Spline curve fits on y-oriented edges (D), which represent fibre tracking.

3.2 Global Organisation

Determining the angle of minimum intensity variance across window rotation angles revealed that different window sizes can also reveal different tissue structural features (Figure 3). The histograms show a significant reduction in entropy for the 7x7 (Figure 3(B)) window, compared with the 5x5 (Figure 3(A)) and 9x9 (Figure 3(C)) window. Two orthogonal angles, 45° and 135°, dominate the 7x7 window analysis (Figure 3(E)), and correspond to global u and v tissue parameters. Therefore, the 7x7 window analysis provides an appropriate standard for normal tissue.

3.3 ECM Quantification of Normal and Enzyme-Digested Tendon

MR images, NIR-MPLSM images and quantification results are compared in normal and digest samples (Figure 4). MRI can identify macroscopic changes to the tendon: PBS-treated tendon appears normal; papain and trypsin induced moderate damage; and collagenase caused severe identifiable damage. SHG images showed disrupted ECM in enzyme-digested tendon samples. Papain and collagenase alter crimp waveform parameters, while trypsin-induced damage

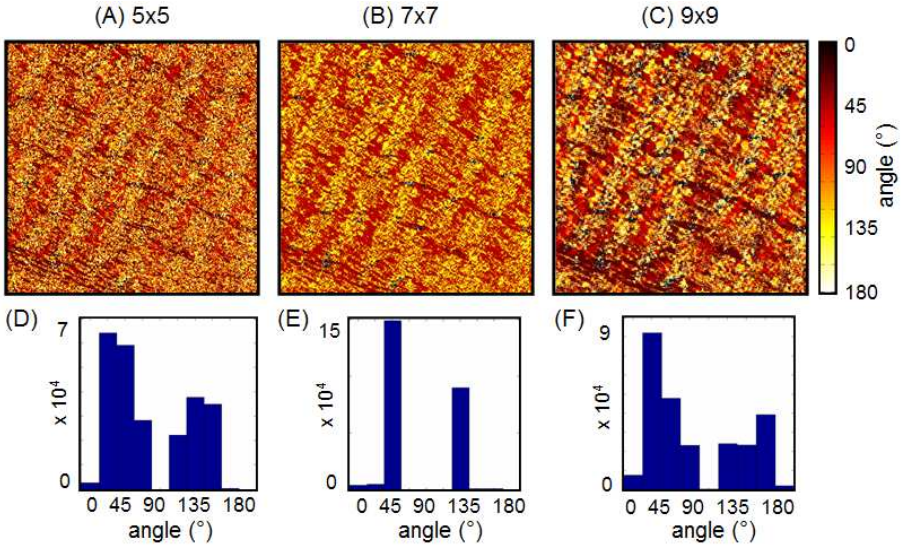

Figure 3. Upper panels show image angles of least variance for different window sizes: (A) 5x5, (B) 7x7, and (C) 9x9 window. Lower panels show the corresponding histograms. The corresponding raw image is shown in Figure 1(C).

seems to manifest between the fibre bundles. Merged images show that enzyme digestion reduces the amount of CS-56 present between the collagen fibres, and in particular trypsin allowed only vascular CS to remain intact. Spline curves representing crimping are merged with the SHG and CS-56 images. The 7x7 window analysis of the global geometry shows that two orthogonal angles, $45°$ and $135°$, dominate the 7x7 window analysis for normal tendon only; histograms reveal that the angle distributions for digested tendon do not contain distinct peaks.

The most striking result from ECM quantification is that digested sample crimp amplitudes, A, were approximately half of that of the the normal sample (Table 1). Tissue curvature, κ, was consistently reduced by digestion, possibly attributed to breaking of collagen cross-links or reduction in CS. Papain- and trypsin-digested sample crimp wavelengths, λ, increased compared to the normal tissue, and trypsin digestion decreased the number of tissue edges (splines). Finally, the order, Δ, of the tendon samples was dramatically reduced by digestion.

Incubation	No splines	A (μm)	λ (μm)	κ	Δ
PBS	222	5.12	32.9	0.0405	1.00
Papain	208	2.77	42.9	0.0266	0.530
Trypsin	145	3.87	37.5	0.0311	0.592
Collagenase	192	2.76	32.7	0.0347	0.719

Table 1. Quantification (mean values) for normal (PBS-incubated) and enzyme-digested samples. No splines is number of splines; A is amplitude; λ is wavelength; κ is curvature; and Δ is order.

One limitations of this study is the small sample size, and the invariable enzyme concentration and incubation time. Further work includes a range of such variables in order to attain imaging standards for a wide range of quantifiable damage. Another limitation is . Finally, the difficulty in translating this work *in vivo* will need to be overcome in order to make it clinically viable. Although clinical ultra-high field MRI scanners are currently rare, they are becoming more widespread and there are alternative methods (such as contrast agents and UTE), which enhance tendon signal.

4 Conclusion

This study shows for the first time that MRI and NIR-MPLSM can reveal complementary and corresponding physiological tendon properties at different and comparable scales; both modalities were able to distinguish between normal and enzyme-digested tendon. The novel NIR-MPLSM image analysis method enabled quantification of the matrix regularity, crimp waveform and GAG spatial distribution, three of several physiological parameters known to be linked to tendon biomechanical properties. This combination of state of the art imaging techniques across imaging modalities, matrix biology and image analysis has presented a unique opportunity for functional investigation of tendon tissue, with potential for translation to an *in vivo* imaging tool, for clinically assessing injury, disease and repair.

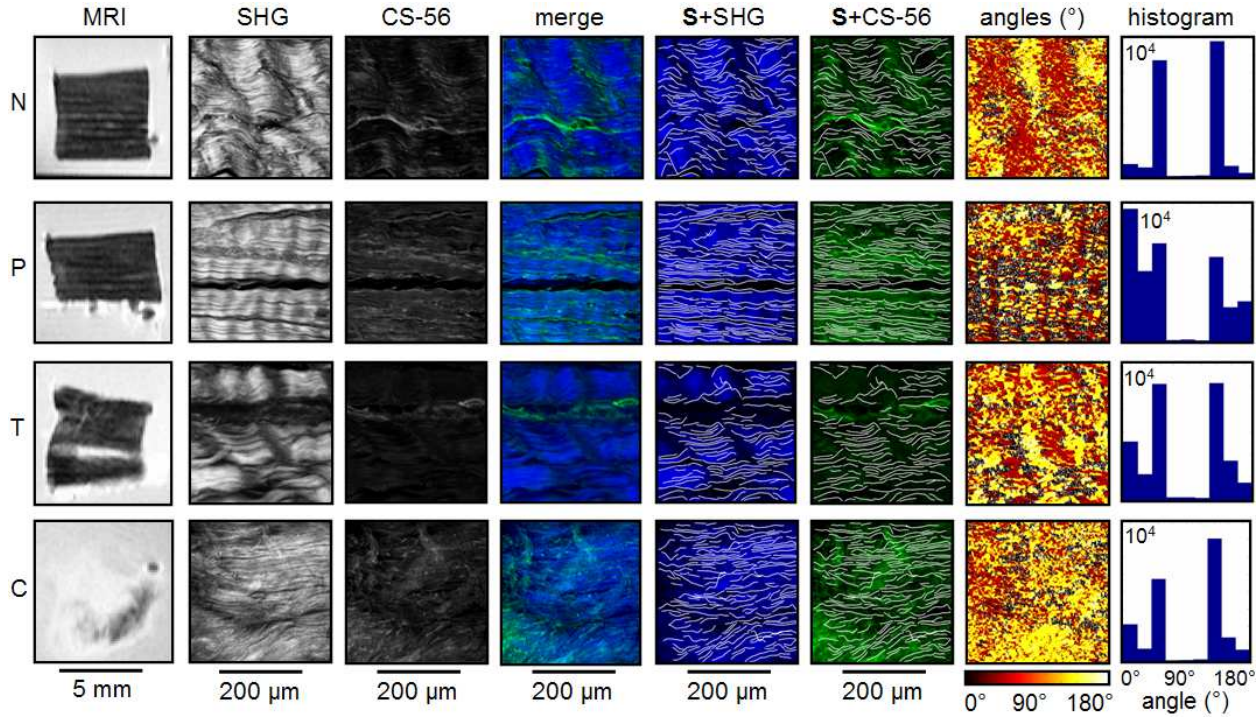

Figure 4. MR images and NIR-MPLSM images of PBS-incubated and enzyme-digested tendon samples. SHG and CS-56 columns present raw signal intensities. The merge column shows SHG (blue) and CS-56 (green) superimposed. **S**+SHG and **S**+CS-56 columns show spatial distributions of the splines relative to the SHG and CS-56 signals. Angles and histogram columns show 7×7 global analysis and corresponding histograms. The ECM and crimp waveform regularity is disrupted in the enzyme-digested tendon samples relative to the normal tendon sample. N - normal (PBS); P - papain; T - trypsin; C - collagenase.

Acknowledgements

The authors would like to thank: Paul A. Raju, Uday Tirlapur and Clarence Yapp for their contributions in NIR-MPLSM image acquisition; Lowri Cochlin for her help with the MR imaging; and Philippa A. Hulley and Hannah R. Cornell for their advice in sample preparation and immunohistochemistry. Ann K. Harvey is funded by the EPSRC-led Life Sciences Interface Doctoral Training Centre.

References

1. K. Miyasaka, D. Daniel, M. Stone et al. "The incidence of knee ligament injuries in the general population." *Am J Knee Surg* **(4)**, pp. 3–8, 1991.
2. R. S. Wolf & L. J. Lemak. "Revision anterior cruciate ligament reconstruction surgery." *J South Orthop Assoc* **11(1)**, pp. 25–32, 2002. 1059-1052 (Print) Journal Article Review.
3. D. Amiel, J. B. Kleiner, R. D. Roux et al. "The phenomenon of "ligamentization": anterior cruciate ligament reconstruction with autogenous patellar tendon." *J Orthop Res* **4(2)**, pp. 162–172, 1986.
4. P. Kannus. "Structure of the tendon connective tissue." *Scandinavian Journal of Medicine and Science in Sports* **10(6)**, pp. 312–320, 2000.
5. A. K. Harvey, M. S. Thompson, L. E. Cochlin et al. "Funtional imaging of tendon." In S. McKenna & J. Hoey (editors), *Medical Image Understanding and Analysis*. Proc. of the 12th Ann. Conf., Dundee, 2008.
6. J. Canny. "A computational approach to edge detection." *IEEE PAMI* **8(6)**, pp. 679–698, 1986.
7. M. P. do Carmo. *Differential Geometry of Curves and Surfaces*. Prentice Hall, New Jersey, 1976.